The Structural and Thermodynamic Analysis of Phase Formation Processes in Equiatomic AlCoCuFeNiCr High-Entropy Alloys

M. Dufanets, V. Sklyarchuk, Yu. Plevachuk (ID), Y. Kulyk, and S. Mudry

Phase formation processes in equiatomic AlCoCuFeNiCr high-entropy alloys have been studied by means of x-ray diffraction method, microstructure analysis and microhardness measurements. Thermodynamic and structural criteria for predicting the phase composition of the alloys were considered. It is shown that in AlCoCuFe, AlCoCuFeNi and AlCoCuFeNiCr alloys the two-phase mixture of solid solutions on the base of the BCC and FCC lattices is formed. With a decrease in the fraction of Al atoms, the tendency to disordering of BCC solid solution occurs. It was also established that alloys under investigation reveal a dendritic structure in which Cu-enriched FCC phase is deposited in the regions between the dendrites of the main BCC phase. The correlation between microhardness of the alloys and volume fractions of phase constituents and their thermodynamic characteristics are revealed.

1. Introduction

Recently, the significant fundamental and applied interest began to be shown in multicomponent alloys, in which content of each constituent element is equal. The entropy of such alloys increases with increasing number of elements and is close to ideal entropy of a multicomponent solution. Due to a high value of the entropy of mixing, there is a possibility to high thermodynamic stability of disordered atomic solutions (Ref 1-3). Experimental studies showed evidently that high-entropy alloys (HEAs) have unique physicochemical and mechanical properties, such as high hardness, wear resistance, thermal stability and corrosive resistance. Such alloys can combine strength (Ref 4), stability to softening (Ref 5) and plasticity (Ref 6) that allows to use them as tools in machine building industry and metallurgy. However, it should be noted that in many HEAs the formation of solid solutions occurs (Ref 2, 7) and their deposition during solidification is the main reason of degradation of the mechanical properties. It is obvious that high entropy of mixing is not only one and sufficient criterion for HEA formation condition. For this reason, it is important to find and apply another criterion for controlled processes of the formation of alloys with desired structure. The results of experimental studies allowed to conclude that phase formation during HEA solidification depends significantly on difference of atomic radii of constituent elements, their electron concentration and thermodynamic parameters. But it should be noted

that to date there is no criterion for controlled formation of the desired structure, with the optimal combination of different mechanical characteristics. In addition, among the HEAs in which solid solutions are formed, alloys consisting of a mixture of BCC and FCC phases are of considerable interest (Ref 8, 9). Alloys such as CoFeNiCr, doped with Al and Cu, demonstrate the best combination of hardness, strength and corrosive resistance. Unfortunately, due to the possibility of the formation of intermetallic compounds, the available information on phase formation in these alloys is quite contradictory (Ref 1, 7). For this reason, it is necessary to conduct further investigations of the structure and physical properties. In this study, the results of experimental evaluation of structure, microstructure and mechanical properties of a few equiatomic HEAs of AlCuNiFeCoCr system of different chemical composition are presented. Special attention is paid to the analysis of structural and thermodynamic criteria for the formation of different phases and their content both affecting the mechanical properties of the alloys.

2. Experimental Details

Samples of HEAs under investigation with concentrations, corresponding to AlCoCuFe (1), AlCoCuFeNi (2), AlCoCuFeNiCr (3) and CoCuFeNiCr (4) stoichiometry and mass of 25 g have been obtained by arc melting method in argon atmosphere. Melting was carried out in the copper crucible, cooled by water, and with a help of the molybdenum electrode. The purity of constituent elements was not less than 99.9%. In order to obtain the samples of high homogenization, they were remelted 4-5 times and then cooled to room temperature with a rate of 50-100 K/s. s. X-ray diffraction (XRD) studies have been carried out by means of DRON-3 diffractometer (Co-K$_{\alpha}$-radiation, graphite monochromator, installed in diffracted beam).

The structure parameters (peak positions and half-width, cell parameters of high precision, determination of subpeaks from

M. Dufanets, V. Sklyarchuk, Yu. Plevachuk, Y. Kulyk, and S. Mudry, Department of Metal Physics, Ivan Franko National University of Lviv, Kyrylo & Mephodiy Str. 8, Lviv 79005, Ukraine. Contact e-mail: plevachuk@mail.lviv.ua.

complex diffraction maxima) have been obtained from diffraction patterns using DHN_PDS software (Włodzimierz Trzebiatowski Institute of Low Temperature and Structure Research of Polish Academy of Sciences, Wroclaw, Poland). The values of the relative microdeformation of the crystalline cell were calculated by the Stock–Wilson method (Ref [10]):

$$\varepsilon = \frac{\beta}{4tg(\theta)}, \tag{Eq 1}$$

where β is the expansion of diffraction maximum caused by microdeformation of crystalline cell and 2θ is the diffraction maximum position. The error in determining the relative deformation of the lattice did not exceed 5%.

Volume fractions of BCC and FCC phases have been estimated comparing relative intensities of diffraction peaks for (220) FCC (γ) and (211) BCC (α) phases using the following formula:

$$X_\alpha = \frac{I_{(211)\alpha}}{I_{(211)\alpha} + I_{(220)\gamma}}, \quad X_\gamma = \frac{I_{(220)\gamma}}{I_{(211)\alpha} + I_{(220)\gamma}} \tag{Eq 2}$$

Microstructure of polished samples was investigated with the help of scanning electron microscope REM-1061, equipped with energy-dispersive x-ray spectrometer (EDS) system and giving a possibility to carry out the local chemical analysis of various phases in the alloy with a resolution of 1 μm. Microhardness was measured by means of PMT-3 setup under loading 1.65 N according to the standard method, similar to the procedure described in Ref [11].

3. Results and Discussion

In our previous study, structure, microstructure and mechanical properties for selected 4- and 5-component equiatomic alloys of AlCuNiFeCoCr system were studied (Ref [12]). Some data obtained in Ref [12] are used in the present work for comparison. As shown in Fig. 1(a), the diffraction pattern for AlCoFeCu alloy, marked as **1**, reveals two sets of diffraction maxima, which correspond to ordered solid solution with BCC lattice (structure type B2) and solid solution with FCC lattice (structure type A1). Existence of atomic ordering is confirmed by the presence of a slight superstructure maximum (100) at $2\theta \approx 37°$ (Fig. 2a). The microstructure of the alloy shows the
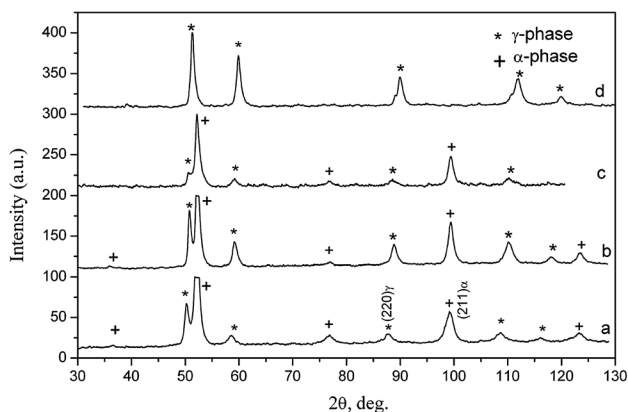
dendrite kind structure (Fig. 5a). According to the results of the local chemical analysis (Table [1]), a dendrite phase is Fe and Co atoms enriched ($\sim$ 30 at.%) and it is ordered BCC phase. The light regions, corresponding to the FCC solid solution, are formed in interdendritic regions, and they present Cu-enriched solid solution (78 at.%), which also consists of 12 at.% Al, 5 at.% Fe and 5 at.% Co.

The procedure of diffraction pattern mathematical interpretation for the alloy **1** within angular range $2\theta = 85°-30°$ by means of DHN_PDS software is shown in Fig. 3. Experimental intensity values, corrected for background scattering, are presented as superposition of separated peaks. The intensity of background scattering is approximated by a linear function. The profile of diffraction maxima is interpreted by means of the Lorentz function:

$$I(2\theta_i) = \frac{I_{max}}{\left\{ 1 + 4\ln(2)\frac{(2\theta_i - 2\theta_{max})^2}{\beta^2} \right\}}, \tag{Eq 3}$$

where I_{max} is the maximum intensity of the diffraction peak and $2\theta_{max}$ is its angular position. The diffraction pattern was calculated as an additive sum of single peaks, and the difference between experimental and calculated patterns allowed us to calculate the discrepancy factor:

$$Rp = \frac{\sum \{I_{exp.}(2\theta_i) - I_{calc.}(2\theta_i)\}}{\sum I_{exp.}(2\theta_i)} \tag{Eq 4}$$

where $I_{exp.}(2\theta_i), I_{calc.}(2\theta_i)$ are experimental and calculated intensity, respectively. As shown in Fig. 3, the discrepancy factor for considered range of diffraction pattern does not exceed 2.2%.

As a result of diffraction data analysis, it was revealed the significant increase in cell parameter for FCC phase in comparison with pure Cu ($a \approx 3.65$ Å) and occurrence of a significant deformation of phases with both crystalline lattices, namely FCC (0.2%) and BCC (0.24%) (Table [2]). The analysis of a half-width of diffraction maxima confirms the existence of significant distortions of a crystalline cell. Particularly, the notable peak broadening for (220) BCC and (222) FCC phases in comparison with reflexes (110) BCC and (111) FCC phases has been revealed. Taking into account the instrumental broadening, the relation between the half-width and the scattering angle is $\frac{\beta_2}{\beta_1} \approx \frac{tg(\theta_2)}{tg(\theta_1)}$ that indicates the dominant

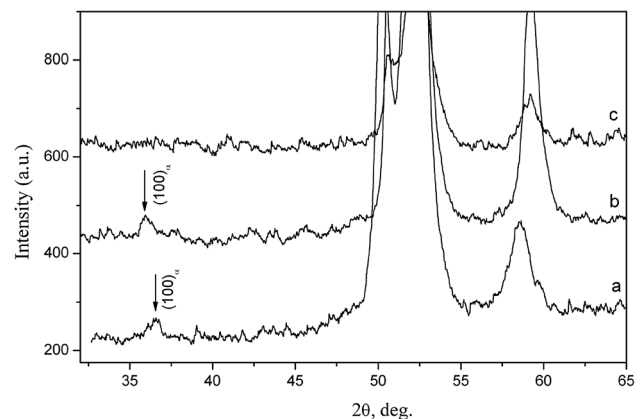**Fig. 1** X-ray diffraction patterns of high-entropy alloys. (a) AlCoCuFe, (b) AlCoCuFeNi, (c) AlCoCuFeNiCr, (d) CoCuFeNiCr

Fig. 2 X-ray diffraction patterns, obtained within $2\theta = 30°-65°$ angular range. (a) AlCoCuFe, (b) AlCoCuFeNi, (c) AlCoCuFeNiCr

Table 1 Phase and chemical composition of HEAs from local chemical analysis (EDS)

No.	Alloy	Chemical composition, at.%						Phase	a, Å	ε, %
		Al	Ni	Co	Cu	Fe	Cr			
1	AlCoCuFe	10.6	…	5.6	78.9	4.9	…	FCC	3.6525	0.20
		20.0	…	34.3	13.8	31.9	…	BCC	2.8790	0.24
2	AlCoCuFeNi	9.2	19.9	18.2	36.5	16.2	…	FCC	3.6195	0.12
		13.5	22.8	23.9	17.6	22.2	…	BCC	2.8739	0.07
3	AlCoCuFeNiCr	10.0	13.3	5.4	62.9	5.0	3.4	FCC	3.6232	0.20
		12.4	19.4	19.1	19.6	17.4	12.0	BCC	2.8741	0.02
4	CoCuFeNiCr	…	11.0	3.3	78.7	3.8	3.1	FCC (γ_1)	3.6085	…
		…	21.0	23.9	9.7	22.0	23.4	FCC (γ_2)	3.5824	0.04
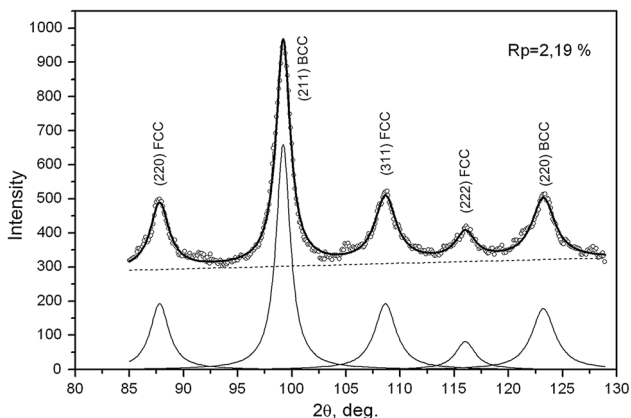
Fig. 3 The interpretation of x-ray diffraction patterns for AlCoCuFe alloy by means of DHN_PDS software (° denotes experimental values of intensity, solid curve is a calculated scattered intensity, dash-dotted curve is a background scattering, at the bottom of the figure the profiles of individual peaks are shown)

Table 2 Phase composition of HEAs from XRD analysis

No.	Alloy	Phase	a, Å	ε, %	X, %
1	AlCoCuFe	FCC	3.6525 ± 0.0016	0.20	23.0
		BCC	2.8790 ± 0.0023	0.24	77.0
2	AlCoCuFeNi	FCC	3.6195 ± 0.0014	0.12	34.0
		BCC	2.8739 ± 0.0016	0.07	66.0
3	AlCoCuFeNiCr	FCC	3.6232 ± 0.0018	0.20	17.0
		BCC	2.8741 ± 0.0010	0.02	83.0
4	CoCuFeNiCr	FCC (γ_1)	3.6085 ± 0.0013	–	29.0
		FCC (γ_2)	3.5824 ± 0.0009	0.04	71.0

contribution of microdeformation of the crystalline lattice of the solid solution into broadening of peaks. This kind of distortion appears due to diluting of atoms with different atomic radii. It can be supposed that the main reason of such structural changes is the presence of Al atoms of larger size in the solid solutions.

We will consider the structure changes that occur when Ni atoms are added to the alloy **1** up to the equiatomic composition. Similarly, diffraction pattern formed in AlCoCuFeNi (**2**) alloy (Fig. 1b) has two sets of diffraction peaks, corresponding to ordered BCC (structure type B2) and FCC (structure type A1) phases. It should be noted that the increase in the volume fraction of FCC phase is well distinguished as the

dark (dendrite) and light (interdendritic) regions for the alloy **2** (Ref 12).

The results of chemical analysis for the above-mentioned structural components (Table 1) show that the dark regions, enriched with Fe, Co and Ni atoms, correspond to the ordered BCC phase (Fig. 2b). On the contrary, light regions indicate a high content of Cu atoms (36.5 at.%) and correspond to the solid solution with FCC lattice. From the analysis of diffraction data of the alloy 2, a slight increase in the cell parameter for the FCC phase was revealed, as compared to pure copper ($a \approx 3.62$ Å) and it was caused from the dissolution of Al to about 9 at.% (Table 2). On the other hand, the reduced cell parameter of alloy **1** is related to a decrease in the Cu concentration in solution and an increase in the amounts of transition elements (Fe, Co, Ni) with less atomic radius. A cell parameter for the ordered BCC phase has an intermediate value between cell parameters of ordered phases NiAl ($a = 0.2887$ nm) and CoAl ($a = 0.2867$ nm), which represent the structure type B2. It is also important that most large values of lattice relative deformation are observed for disordered solution on the base of the FCC phase (0.12%) because of significant difference between atomic radius of Al and other elements. At the same time, the relative lattice deformation for the BCC phase is about twice less (0.07%) that can be explained by a decrease in the Al atoms fraction in solid solution of BCC phase (see Table 1).

The results of the x-ray phase analysis (Fig. 1c) show the formation of two-phase structure in the six-component AlCoFeCuNiCr (**3**) alloy too. The diffraction pattern reveals two sets of maxima from disordered solutions with BCC (type B1) and FCC (type A1) lattices. But the intensity of peaks for FCC phase is notably less, indicating the decrease in its volume fraction (Table 2). The increase in BCC phase fraction is supposed to be caused by the presence of Cr in the alloy, which is possessed by BCC-type structure that has the highest melting temperature (2180 K̇) in comparison with other constituent elements. The results of chemical analysis revealed that BCC phase contains up to 75 at.% of transition elements (Fe, Co, Ni, Cr), 12 at.% Al and 12 at.% Cu. It can be supposed that disordering of the BCC solid solution and disappearing of a superstructure maximum (100) are caused by high content of transition metals in the solid solution (Fig. 2c). It should also be noted that a microstructure of the alloys **1** and **2** is of a dendrite kind (Fig. 5c). Dark regions correspond to grains of BCC phase, whereas the light regions correspond to Cu-enriched (63 at.%) solid solution with the FCC cell, and it is located between the grains of the BCC phase (Ref 12). In comparison

with pure Cu, there is some increase in the cell parameter and the relative lattice deformation reached 0.2% that is proved by significant smearing of maxima, corresponding to FCC phase. At the same time, the microdeformations in the BCC phase are notably less (0.024%) that most probably is caused by large concentration (~ 75 at.%) of transition elements in the solid solution of the BCC phase.

Diffraction pattern for the CoFeCuNiCr alloy (**4**) (Fig. 1d) reveals intensive peaks (111), (200), (220), (311), (222), which correspond to disordered solid solution with FCC cell. But in this case the diffraction pattern has additional peaks in the vicinity of (220) and (311) peaks (Fig. 4). Thus, it is possible to suppose that these peaks correspond to another solid solution with the same type of crystalline lattice and similar value of cell parameter. The confirmation of such supposition is the presence of deposited one phase (light color) between crystallites of another phase, whose content is significantly larger (Fig. 5d). Analysis of chemical composition of structural constituents allowed to reveal that the phase (γ_2) was depleted with Cu (9 at.%) at almost the same content of other elements (21-23 at.%). Copper-enriched phase (γ_1), containing about 79 at.% Cu and 11 at.% Ni, is depleted with Fe, Co and Cr (3-4 at.%). As seen, the results of microstructure analysis correlate satisfactory with XRD data. A cell parameter of the phase is less than one for pure Cu on the reason that the solid solution is enriched with transition elements (Ni, Fe, Co and Cr), which have lower atomic radii (Table 1). On the same reason, we have observed the low value of lattice microdeformation (0.024%) for base (γ_2) FCC phase (Table 2). Cell parameter of Cu-enriched solid solution (γ_1-phase) also becomes lower comparatively to pure Cu due to substitution of some Cu atoms by atoms of elements with lower atomic radii.

In order to find the correlation between atomic structure and phase characteristics of HEA with their mechanical properties, the measurements of microhardness have been carried out (Table 3). As follows from experimental results, there is some correspondence of such characteristic with a phase content of an alloy. Particularly, alloy **4**, containing the highest amount of FCC phase, has the lowest microhardness ($H_V \approx 2.7$ GPa). Besides, it is known that plasticity of crystals with FCC cell is higher, whereas the hardness is lower than in BCC crystals. Such feature is caused by the fact that planes of sliding {111} of the FCC phase have higher density of atomic packing comparatively to ones of the {110} BCC phase that results in
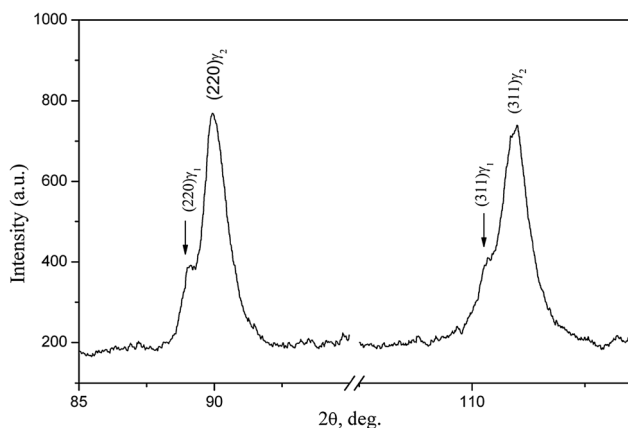

Fig. 4 Profile of (220) and (311) x-ray diffraction peaks for CoCuFeNiCr alloy

lower resistance at plastic deformation process. The increase in fraction of solid solution with a BCC lattice (Table 4) leads to an increase in the microhardness from 4.6 to 5.9 GPa in the alloys **2**, **1** and **3**.

According to the results of the structural characterization of HEAs (Ref 9), the continuous solid solution formation is reached due to high entropy of mixing. It is accepted that high values of the entropy of mixing avoid the formation of intermetallics and ordered solid solutions. For calculation of the entropy of mixing, a well-known formula is commonly used:

$$\Delta S = -R \sum_i c_i \ln(c_i), \qquad \text{(Eq 5)}$$

where $R = 8.31$ J/K mol is the gas constant and c_i is the atomic fraction of ith component of an alloy.

The results of such calculations for alloys under investigation are listed in Table 2 and show that the highest ΔS value corresponds to the alloy with a maximum number of components (alloy **3**, in our case). But from the results of phase analysis of this alloy, the two-phase structure as a mixture of FCC and BCC phases is also formed. Therefore, the phase content of HEA should be determined not only by entropy of mixing but also from physical and chemical characteristics of constituent components. Another thermodynamic characteristic, whose values have an influence on the process of the solid solution formation in HEA, is the enthalpy of mixing, which is commonly calculated according to formula:

$$\Delta H = 4 \sum_{i,j} c_i c_j \Omega_{ij}, \quad \Omega_{ij} = 4\Delta H_{ij} \qquad \text{(Eq 6)}$$

where ΔH_{ij} is the partial entropy of mixing for ith and jth components of an alloy. Thermodynamic criterion, which allows to predict approximately the phase content of HEA, can be estimated as

$$\Omega = \left| \frac{T_L \Delta S}{\Delta H} \right|, \qquad \text{(Eq 7)}$$

where $T_L = \sum_i c_i T$ is the mean melting temperature.

Analysis of these thermodynamic factors for some HEAs (Ref 13, 14) allowed to establish that the formation of solid solutions occurs in such cases when enthalpy of mixing varies within a range of $-15 \leq \Delta H \leq 5$ kJ/mol, and thermodynamic criterion Ω is not less than 1,1. It can be seen that ΔH and Ω values lie within the ranges, which correspond to conditions, needed for the formation of solid solutions (Table 3). For all alloys, with exception of the alloy **4**, the negative value of enthalpy of mixing is observed that is the evidence of strong chemical interactions between constituent elements.

In order to predict the phase content of HEA, it is proposed to consider, beside thermodynamic, the structure criteria too. In disordered solid solutions, all atoms occupy positions in the unit cell with equal probability. Consequently, each atom can be considered as an atom of a diluted substance, which causes the distortion of crystalline lattice due to the atomic radii difference. For description of a complex influence of atomic radii, a difference in the size parameter δ was introduced:

$$\delta = \sqrt{\sum_i c_i \left(1 - \frac{r_i}{\bar{r}}\right)^2} \times 100\%, \qquad \text{(Eq 8)}$$

where r_i is the atomic radii of elements and $\bar{r} = \sum_i c_i r$ is a mean atomic radius of an alloy.
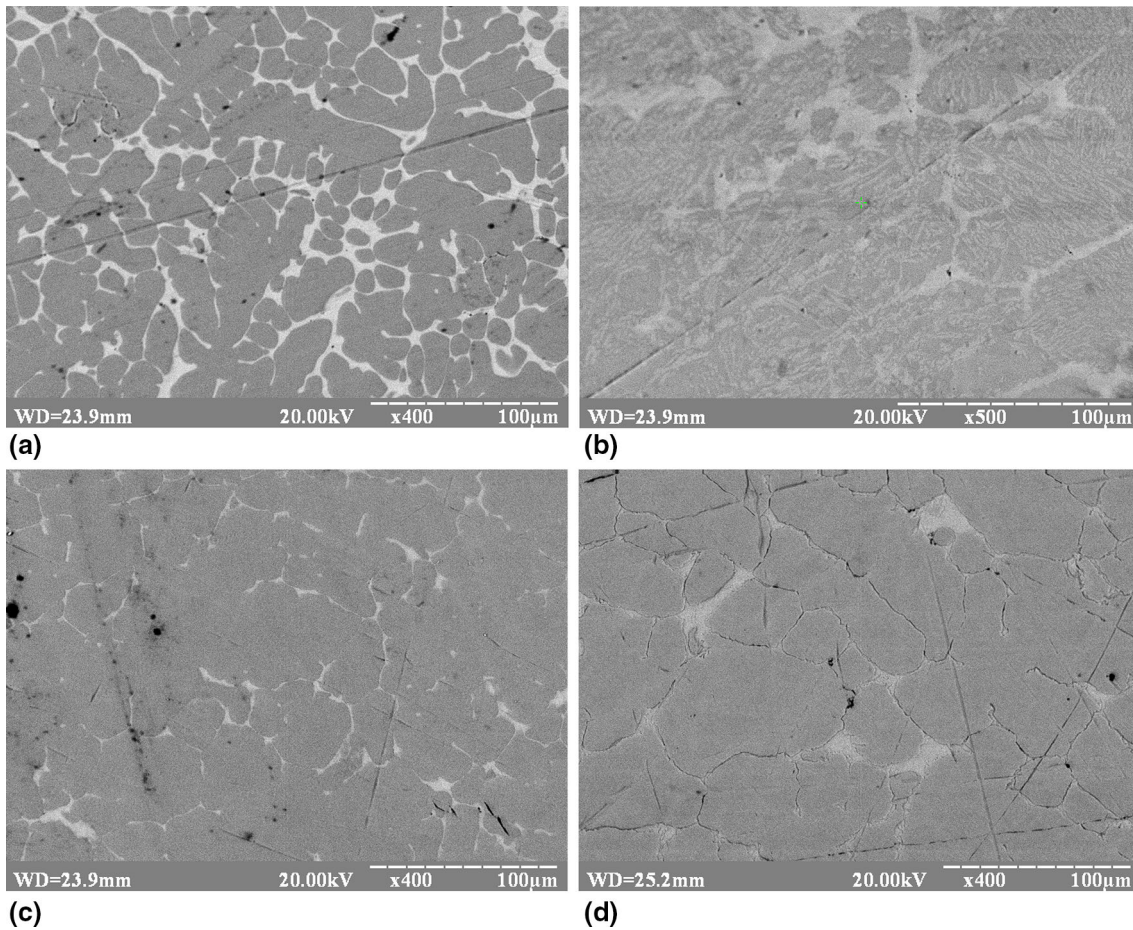
Fig. 5 Comparison of SEM images of high-entropy alloys. (a) AlCoCuFe (Ref 11), (b) AlCoCuFeNi (Ref 11), (c) AlCoCuFeNiCr, (d) CoCuFeNiCr

Table 3 Thermodynamic, structural and mechanical characteristics of HEA of nominal composition

No.	Alloy	ΔS, J/k mol	ΔH, kJ/mol	T_L,.K	Ω	δ, %	H_V, GPa
1	AlCoCuFe	11.52	− 3.25	1466	5.2	5.59	5.45
2	AlCoCuFeNi	13.34	− 5.28	1518	3.8	5.44	4.56
3	AlCoCuFeNiCr	14.86	− 5.62	1631	4.3	5.02	5.93
4	CoCuFeNiCr	13.34	+ 1.92	1767	12.3	1.12	2.74

Table 4 The enthalpy of mixing of binary alloys ΔH_{AB} (kJ/mol)

Element	Al	Co	Cu	Fe	Ni	Cr
Al	...	− 19	− 1	− 11	− 22	− 10
Co	...	...	+ 6	− 2	0	− 4
Cu	...	...	...	+ 13	+ 4	+ 12
Fe	...	...	...	...	− 2	− 1
Ni	...	...	...	...	...	− 7

As shown in Ref 15, the formation of solid solutions and absence of intermetallic and amorphous phases occur at values of δ parameter within interval $1 \leq \delta \leq 6$ %. The formation of the single-phase disordered solid solutions with BCC (FCC) structure is possible at values of its parameter $\delta \leq 4.6$ %($\delta \leq 4.0$ %). In other words, the solution with a BCC cell can be formed at larger atomic radii of components difference. For all alloys, its value is less than 6% that confirms the formation of the solid solutions mixture. Minimum value of the structure parameter is observed for the alloy **4** ($\delta = 1.12$%) that should indicate the formation of the single-phase structure of disordered solution. On the other hand, the structure studies indicate the deposition of Cu-enriched FCC phase in the interdendritic space of a basic phase. A maximum value of parameter δ is reached in the alloy **1** that allows to explain the high inner stresses in both phase constituents of the alloy. Besides, it should be noted that an increase in such parameter promotes the formation of the ordered BCC solid solutions (structure type B2), observed in the alloys **1** and **2**.

Table 5 Thermodynamic and structural characteristics of the phase constituent HEA

No.	Alloy	Phase (structure type)	ΔH, kJ/mol	Ω	T_L, K.	δ, %	X, %
1	AlCoCuFe	BCC (B2)	− 5.14	3.33	1557	5.13	77.1
		FCC (A1)	+ 2.04	4.04	1354	3.65	22.9
2	AlCoCuFeNi	BCC (B2)	− 3.51	5.94	1579	4.76	66.1
		FCC (A1)	+ 1.77	10.92	1537	3.97	33.9
3	AlCoCuFeNiCr	BCC (B1)	− 5.46	4.59	1695	4.53	82.9
		FCC (A1)	+ 1.72	8.42	1434	3.78	17.1
4	CoCuFeNiCr	FCC$_{\gamma 1}$ (A1)	− 0.70	33.9	1825	1.03	71.4
		FCC$_{\gamma 2}$ (A1)	+ 3.80	2.46	1450	0.86	28.6

It is clear that for complete analysis of the phase formation process in multicomponent alloys, the interatomic interaction of components must be taking into account. The degree of such interaction is the thermodynamic characteristic—partial enthalpy of mixing ΔH_{AB} for A-B binary molten alloys. As shown in Table 4, collecting the values of ΔH_{AB} for binaries, the existing Cu in multicomponent alloys results in the significant positive enthalpy of mixing with transition elements, that is, evidence of preferred interaction of the like kind atoms (Ref 16).

Particularly, in sequence from Al to Fe its value varies within a range from − 1 to + 13 kJ/mol that leads to forcing out the Cu atoms into interdendritic spaces at the second stage of crystallization and formation of a solid solution on the base of the FCC lattice. Contrary to Cu, Al shows the strong chemical interaction with transition metals that is manifested by significantly negative values of ΔH_{AB}. As a consequence, the ordering of a solid solution on the base of the BCC phase with structure type B2 is observed in the alloys **1** and **2** with higher content of Al. Similar behavior is also typical for interaction of atoms in Fe-Co, Fe-Ni, Fe-Cr and Cr-Ni melts. On that reason, the initial BCC phase consists of elements with negative pair enthalpy of mixing and its morphology has dendrite features. During dendrite growth, the rest melt enriches with Cu and crystallizes in the interdendritic regions. For confirmation of such assumptions, few thermodynamic characteristics and structure criterion for each phase component have been calculated according to formulas (3, 4) (Table 5).

As seen, the enthalpy of mixing for initial BCC phase is negative for all alloys and the mean melting temperature is, respectively, higher, which is the reason of deposition of this phase from the melt during first stages of transformation. It is of importance that a correlation between ΔH of initial BCC phase and microhardness of the alloy exists. The alloys with more negative enthalpy of mixing show the larger hardness due to an increase in the energy of chemical interaction between the components. At the same time, the Cu-enriched FCC phase has positive ΔH values and lower melting temperature, that is why it is formed at the second stage of crystallization. Special attention should be paid to analysis of a size factor for both phases. In the alloys **1** and **2**, the parameter δ for BCC phase prevails the critical value $\delta = 4.6\%$ for more stability of disordered solid solution. This result can be considered as one of the reasons that lead to atomic ordering in the BCC phase and the formation of superstructure of B2 type. At the same time, the formation of disordered solid solution on the base of the BCC phase occurs for the alloy **3** with $\delta = 4.5\%$. It is also of importance that the size parameter of the FCC phase in the alloys **1-3** approaches the critical value $\delta \approx 4\%$ resulting in

appearance of significant inner stresses. Therefore, the results obtained in this work suggest the possibility of significant influence of the component content variation on structural-phase state and properties of high-entropy alloys.

4. Conclusions

1. In correspondence to thermodynamic and structural criteria and based on x-ray phase and microstructure analysis, it is shown that the structure of the equiatomic high-entropy AlCoCuFeNiCr alloys has two-phase behavior and contains solid solutions with BCC (B1 or B2 structure types) and FCC lattice (A1 structure type).
2. Addition of Al promotes the formation of the BCC phase. Besides, in alloys with higher content of Al the ordering and appearing of superstructure of B2 type is observed. A decrease in the Al content leads to transition to the disordered solid solution (B2 → B1).
3. Initial BCC phase reveals the dendrite morphology and is enriched with transition elements, whereas Cu-enriched BCC solution deposits in the interdendritic regions.
4. The significant variations of microhardness versus volume fraction of phase components and its correlation with thermodynamic characteristics are revealed.

Conflict of interest

On behalf of all authors, the corresponding author states that there is no conflict of interest.

References

1. J.-W. Yeh, S.-K. Chen, S.-J. Lin, J.-Y. Gan, T.-S. Chin, T.-T. Shun, C.-H. Tsau, and S.-Y. Chang, Nanostructured High-Entropy Alloys with Multiple Principle Elements: Novel Alloy Design Concepts and Outcomes, *Adv. Eng. Mater.*, 2004, **6**(8), p 299–303
2. Y.P. Wang, B.Sh. Li, and Zh.F. Heng, Solid Solution or Intermetallics in a High-Entropy Alloy, *Adv. Eng. Mater.*, 2009, **11**(8), p 641–644

3. Yu. Plevachuk, J. Brillo, and A. Yakymovych, AlCoCrCuFeNi Based High-Entropy Alloys: Correlation Between Molar Density and Enthalpy of Mixing in the Liquid State, *Metall. Mater. Trans. A*, 2018, **49**(12), p 6544–6552

4. O.N. Senkov, G.B. Wilks, J.M. Scott, and D.B. Miracle, Mechanical Properties of Nb25Mo25Ta25W25 and V20Nb20Mo20Ta20W20 Refractory High Entropy Alloys, *Intermetallics*, 2011, **11**, p 698–706

5. Y.F. Kao, S.K. Chen, J.H. Sheu, J.T. Lin, W.E. Lin, J.W. Yeh, S.J. Lin, T.H. Liou, and C.W. Wang, Hydrogen Storage Properties of Multi-Principal-Component CoFeMnTixVyZrz Alloys, *Int. J. Hydrog. Energy*, 2010, **35**, p 9046

6. H.-P. Chou, Y.-Sh. Chang, S.-K. Chen, and J.-W. Yeh, Microstructure, Thermophysical and Electrical Properties in AlxCoCrFeNi (0 ≤ x ≤ 2) High-Entropy Alloys, *MatER. Sci. Eng. B*, 2009, **163**, p 184–189

7. S. Singh, N. Wanderka, B.S. Murty, U. Glatzel, and J. Banhart, Decomposition in Multi-component AlCoCrCuFeNi High-Entropy Alloy, *Acta Mater.*, 2011, **59**, p 182–190

8. V.A. Kuznetsov, D.G. Shaysultanov, N.D. Stepanov, G.A. Salishchev, and O.N. Senkov, Superplasticity of AlCoCrCuFeNi High Entropy Alloy, *Mater. Sci. Forum*, 2013, **735**, p 146–151

9. J.W. Yeh, Alloy Design Strategies and Future Trends in High-Entropy Alloys, *JOM-J Min. Met. Mater. Sci.*, 2013, **65**(12), p 1759–1771

10. V.K. Pecharsky and P.Y. Zavalij, *Fundamentals of Powder Diffraction and Structural Characterization of Materials*, Springer, Berlin, 2005, p 713

11. K. Sangwal, B. Surowska, and P. Błaziak, Analysis of the Indentation Size Effect in the Microhardness Measurement of Some Cobalt-Based Alloys, *Mater. Chem. Phys.*, 2002, **77**, p 511–520

12. V. Sklyrchuk, Yu. Plevachuk, M. Dufanets, S. Mudry, and Yu. Kulyk, Structural-phase state of Nanocrystalline Al-based High-Entropy Alloys with Transition Elements, in *Proceedings of the Conference on UKRCON-2019, 2019 IEEE 2nd Ukraine Conference on Electrical and Computer Engineering Lviv, Ukraine. Ukraine Section July 2–6, 2019*, pp. 538–541. https://ieeexplore.ieee.org/document/8879975

13. J.B. Mann, T.L. Meek, and L.C. Allen, Configuration Energies of the Main Group Elements, *J. Am. Chem. Soc.*, 2000, **122**, p 2780–2783

14. S. Ng, C. Guo, J. Lu, and C.T. Liu, Effect of Valence Electron Concentration on Stability of fcc or bcc Phase in High Entropy Alloys, *J. Appl. Phys.*, 2011, **109**, p 103505(1-5)

15. Y. Zhang, Y.J. Zhou, J.P. Lin, G.L. Chen, and P.K. Liaw, Solid-Solution Phase Formation Rules for Multi-component Alloys, *Adv. Eng. Mater.*, 2008, **10**(6), p 534–538

16. A. Takeuchi and A. Inoue, Classification of Bulk Metallic Glasses by Atomic Size Difference, Heat of Mixing and Period of Constituent Elements and Its Application to Characterization of the Main Alloying Element, *Mater. Trans.*, 2005, **46**, p 2817–2829